PNAS
www.pnas.org

Supplementary Information for

ATP allosterically stabilizes Integrin-linked kinase for efficient force generation

Isabel M. Martin, Michele M. Nava, Sara A. Wickström and Frauke Gräter

Frauke Gräter and Sara Wickström.
E-mail: frauke.graeter@h-its.org; sara.wickstrom@helsinki.fi

This PDF file includes:

- Supplementary text
- Figs. S1 to S8 (not allowed for Brief Reports)
- Table S1 (not allowed for Brief Reports)
- Legends for Movies S1 to S13
- SI References

Other supplementary materials for this manuscript include the following:

- Movies S1 to S13

Supporting Information Text

Detailed methods

Equilibrium molecular dynamics simulations. The crystal structures of the human ILK(WT) kinase domain in complex with the CH2-domain of α-parvin either with ATP (Protein Data Bank (PDB)-code 3KMW) or without ATP (3KMU, (1)) were used. To achieve starting structures without parvin, those coordinates were deleted. The PDB-code 6MIB (2) was used for the simulations with the ILK(L207W) mutation. Point mutations for ILK(R225/R349A) were generated using pymol. All MD simulations were carried out using GROMACS 2018.1 (3). The Amber99sb*-ILDNP force-field (4, 5), TIP3-water model (6) and ATP-parameters (7) were used. The starting configurations were solvated in the center of a dodecahedron box with (at least) 3 nm between each periodic image. Sodium and chloride ions corresponding to a physiological concentration of 100 mM were added resulting in a system with overall zero charge. An energy minimization was performed with the steepest descent method, followed by 500 ps in the NVT and 500 ps in the NPT ensemble with harmonic constraints on all protein atoms with a force constant of 1000 kJ mol^{-1} nm^{-1} to equilibrate water and ions. The production runs were carried out in the NPT ensemble without constraints on heavy atoms. All bonds between hydrogens and protein heavy atoms were constrained using the LINCS algorithm (8). Therefore, a timestep of 2 fs could be used. The temperature was kept constant at T = 300 K using the velocity rescaling thermostat (9) with a coupling time of 0.1 ps. The two temperature coupling groups were (1) all protein and ATP atoms and (2) all water and ions. The pressure was kept constant at 1 bar using the isotropic Parrinello-Rhaman barostat (10) with a coupling time of 2 ps and a compressibility of 4.5×10^{-5} bar^{-1}. The neighbors list was updated every 10 fs with the Verlet scheme. A cutoff of 1.0 nm was used for all non-bonded interactions and long-range electrostatic interactions were treated using the Particle mesh Ewald method (PME, (11)) with a grid spacing of 0.16 nm with cubic interpolation. If not stated otherwise the systems were simulated for 500 ns. For the analysis the first 20 ns were neglected as equilibration period, as inspected from the protein backbone root-mean square deviation (RMSD). 20 individual production runs were carried out, with random velocities and their own equilibration phases, totaling to a total simulation time used for the analysis of 9.6 µs per condition.

Guided molecular docking. To determine a patch of residues on ILK that is most likely in contact with kindlin-2 we employed a guided molecular docking approach. One available crystal structure of the nearly complete mouse kindlin-2 is missing only two loops within the F1 domain and the PH-domain (PDB: 5XPY, (12)). Unfortunately, the ILK-binding helix (PDB: 2MSU, (13)) is located at the edge of the PH domain and is only partially included in the nearly full structure. Therefore, we combined all available partial structures of kindlin-2 (ILK-binding helix: 2MSU; free PH-domain: 4F7H and 2LKO (14, 15); N-terminus: 2LGX (16)) and aligned them with the main body of kindlin-2 (PDB: 5XPY) using UCSF-Chimera (17). This structural alignment was performed according to an underlying sequence alignment with the human kindlin-2 generated with T-coffee (18). Since the structures of the free PH-domains do not overlap in sequence with the main kindlin body, they were placed near the artificially inserted loop in the F2 domain of the main body structure in such a way that the residues that follow in the sequence have a minimal distance to each other. In doing so six rotations of the PH-domains were generated. For the missing loop within the F1 domain there is no crystal structure, but it is far apart from the ILK binding site and thus we regard it as neglectable for the ILK binding. The final full structures were generated by a homology modeling using MODELLER (19) based on the positions of the placed fragments. For each of the six conformations, four models were generated. Eleven models in which the F1-loop was not threaded through the protein were selected for further analysis. Those were subjected to a short 20 ns to 30 ns MD simulation (see above for simulation parameters). A cluster analysis over the whole trajectory determined the most populated conformations, which were selected for the guided molecular docking with Haddock2.2 (20). For ILK, the most populated structure from the 100 ns MD simulation of PDB-code 3KMW was used. The experimentally validated residues of ILK that are in direct contact with kindlin-2 (K423, I427, (21)) were chosen as the actively participating residues. The residues of kindlin-2 (L353, E354, L357, E358) that were shown to interact with ILK (13) were set as active residues as well. Passive residues were defined automatically around the active residues. Seven docking protocols were successful and used for further analysis.

Determination of pulling sites. The ILK:kindlin-2 docking poses were used to determine the most physiological cluster of residues for mechanical perturbation. From the 361 highest scoring docking poses we determined the residues in ILK that are in contact with kindlin-2 within a cutoff of 0.35 nm. The residues that occur in most of the docking poses are: P419, H420, K423, I427, K435, M441, K448. These were then taken as the patch of residues for force-probe MD. For parvin, we adopted a similar approach. From the structures of the parvin-CH2 domain in complex with the paxillin LD1 domain (PDB-codes: 4EDN (22) and 2K2R (23)) the residues on parvin that are interacting with paxillin within the same threshold of 0.35 nm were determined. This resulted in the residues A249, T252, V264, T267, R369 as the patch of residues on parvin for pulling.

Force-probe molecular dynamics simulations. We used force-probe MD to simulate the effects of mechanical perturbation on the system. The end-conformations of the equilibrium simulations were placed in the center of a rectangular box of 30 Å $\times$ 15 Å $\times$ 15 Å and rotated so that the axis between the putative pulling points is in line with the x-axis of the box. The system was energy minimized, followed by short simulations in the NVT and NPT ensemble as described above. For the production run the respective residue patches were subjected to harmonic spring potentials with a force constant of 50 kJ mol^{-1} nm^{-1} moving in opposite directions with a constant velocity (v= 1 m s^{-1} to 0.01 m s^{-1}). 10 simulations were performed per velocity and condition. The simulations were stopped upon dissociation of ILK:parvin.

MD analysis and visualization. The computational analysis was performed with GROMACS tools and post-processed with Python 3. If not stated otherwise, the first 20 ns of each equilibrium simulation were excluded from the analysis. The RMSD of the backbone atoms was calculated in relation to the first frame of the production run. Further, the two starting structures of the holo and apo complex were

found to be remarkably similar to each other (1). Thus, the differences in RMSD do not reflect differences in the overall structure of the ILK pseudokinase domain but rather show that ATP influences the dynamical behavior. The saltbridge occupancy/residue contact probabilities were calculated by determining the number of frames of the whole trajectory with a residue-residue distance below a threshold of 0.35 nm. To determine the interface area between ILK and parvin, we calculated the solvent accessible surface area (SASA, (24)) for both proteins alone and for the complex. The interface area can be calculated according to equation 1:

$$\frac{1}{2}(\mathtt{SASA}_{\mathtt{ILK}} + \mathtt{SASA}_{\mathtt{parvin}} - \mathtt{SASA}_{\mathtt{complex}}) \quad [1]$$

We define a complex dissociation event if the interface area is below 0.6 nm. For visualization of protein structures we used visual molecular dynamics (VMD; (25)). For the generation of the final figures we used Inkscape.

Principle component analysis. We performed principle component analysis (PCA, reviewed in (26)) with GROMACS utilities covar and anaeig to identify the major correlated structural motions. The first 20 ns of each equilibrium MD trajectory were neglected and the PCA was conducted on the C-α atoms of the cumulative trajectories of the ILK holo und apo state or ILK(L207W). Rotational and translational motions were removed by superimposing the structures along the trajectory onto the invariant core. A covariance matrix from the C-α positions was generated. The eigenvectors that describe the direction of motion, are generated by diagonalization of the covariance matrix. The corresponding eigenvalue describes the magnitude (energetic contribution) of that component to the motion. Projection of the trajectory on the eigenvectors shows the motions of the protein along this mode of motion. All trajectories were projected onto the eigenvectors generated by the apo state. The top two eigenvectors were considered to construct the two-dimensional histogram.

Force distribution analysis. We used force distribution analysis (FDA (27)) implemented into GROMACS to calculate the changes in internal forces between the ILK holo and apo states. In FDA the pairwise forces between atom pair i and j are calculated considering all interaction types between protein atoms. These time-averaged pairwise forces can be non-zero even in equilibrium simulations. For a residue based analysis the inter-residue forces were calculated according to equation 2:

$$F_{u,v} = \sum_{i \epsilon u, j \epsilon v} F_{ij} \quad [2]$$

where i is an atom of residue u and j is an atom of residue v, with u and v being different and where F_{ij} is the pairwise force between atoms i and j. The FDA was performed on each individual trajectory per condition and the resulting average forces of the apo state were subtracted from those of the holo state. The networks shown are connected edges for at least 3 residues with force differences above a given threshold. Each interaction in the graphs shows a statistically significant change in internal forces (Mann-Whitney test, p <0.05).

The punctual stress is the sum of the absolute values of scalar pairwise forces acting on each atom i:

$$S_i = \sum_j |F_{ji}| \quad [3]$$

Plasmid constructs. Full length mouse ILK cDNA was cloned into the EcoRI site of pEGFP-N1 plasmid (Clontech). The R255A, R349A, and L207W mutations were generated by performing site-directed mutagenesis PCR using Quik Change II Mutagenesis Kit (Agilent) with the following primers:

R255A forward: 5'-CCTTGTACTCCAGTCTGCAACCTTCAGCACCTTCA-3' and
R255A reverse 5'-TGAAGGTGCTGAAGGTTGCAGACTGGAGTACAAGG-3';
R349A forward 5'-AGGCGCATACATGGCCCCAGGGCACTGG-3' and
R349A reverse 5'-CCAGTGCCCTGGGGCCATGTATGCGCCT-3';
L207W forward: 5'-CCTGCCAGCGGCCTTTCCACCACTCTCCAGAATGATTCTCA-3' and
L207W reverse 5'-TGAGAATCATTCTGGAGAGTGGTGGAAAGGCCGCTGGCAGG-3'.

Cell culture and transfection. Immortalized ILK-/- mouse fibroblasts were obtained as described (28) and cultured in Dulbecco's MEM, 10 % FBS (Gibco) in 5 % CO_2 at 37 °C. Transient transfections were performed using Lipofectamine 3000 reagent (Invitrogen) according to the manufacturer's instructions. After 24 h of transfection cells were subjected to specific experimental analyses.

Immunoprecipitation. Transfected cells grown on polystyrene dishes were rinsed in phosphate-buffered saline (PBS), suspended in lysis buffer (50 mM Tris–HCl buffer (pH 8.0) containing 150 mM NaCl, 1 % Triton-X 100, 0.05 % sodium deoxycholate, 10 mM EDTA, protease, and phosphatase inhibitors (Roche)), and cleared by centrifugation. GFP immunoprecipitation was performed using Miltenyi Biotec MultiMACS GFP Isolation Kit (Mylteni Biotec 130-091-125) according to the manufacturer's protocol. The immunocomplexes were eluted in Laemmli sample buffer by boiling and analyzed by western blotting.

Western Blotting. Lysates were reduced in Laemmli sample buffer at 95 °C, separated by PAGE in the presence of SDS, transferred onto PVDF membranes and subjected to western blot analyses using the standard protocols. The following antibodies were used: anti-α parvin (Cell Signalling; 4026 ; 1:2500), anti-GFP (Invitrogen; A1112; 1:2500) and anti-rabbit HRP (Bio-Rad Laboratories). Western blots were quantified using densitometry (ImageJ software) (29) from four independent experiments.

Generation of soft and stiff substrates. 8 kPa and 40 kPa polyacrylamide (PAA) gels (7.5 % acrylamide/0.25 % bis-acrylamide) were cast on 20 x 20 glass coverslips after which fibronectin was chemically crosslinked on gels using Sulfo-SANPAH (Pierce). Gel stiffness was measured as described (30). For traction force microscope gels were manufactured as above by additioning 0.2 µm fluorescent beads (1:125; Polysciences). Gels were washed in 70 % Ethanol and rinsed extensively in PBS after which transfected cells were plated, allowed to adhere and live imaged for focal adhesion dynamic analysis or used for traction force microscopy experiments.

Focal adhesion dynamics. Transfected cells on 8 kPa and 40 kPa Fibronectin-coated PAA gels were imaged using a Zeiss Axiovert inverted microscope coupled to a CSUX1 spinning-disc device (Yokogawa) equipped with a 488 nm laser, sCMOS camera (Hamamatsu) and an environment chamber. Imaging was performed with a 100×oil immersion objective (Zeiss) at 37 °C, 5 % CO_2. Images were acquired at a frame rate of 1 frame/30 sec for 30 min. To quantify adhesion dynamics, time-lapse movies were preprocessed using Fiji (29) by subtracting the background, denoising and linear contrast enhancement. Image sequences were then submitted to Focal Adhesion Server Analysis FAAS (31). The following settings were used: no median filter was applied, detection threshold was set to 2.5. The minimal size for focal adhesion detection, namely the focal adhesion threshold area was set to 20 pixels after a careful visual inspection of the focal adhesion segmentation and tracking. The number of focal adhesions per cell was then normalized to the corresponding cell area. To this purpose, cell edges were manually traced. Assembly and disassembly events per adhesion per cell were collected based on R^2 values greater or equal 0.8 (31).

Traction Force Microscopy. Traction force microscopy was performed essentially as described (32). Transfected cells were cultured on 8 kPa PAA. Imaging was performed using a spinning disc microscope described above with a 40x glycerol objective at 37 °C with 5 % CO_2. Cells were imaged prior and after the addition of 10X trypsin to detach cells and obtain bead displacement images. Calculation of traction forces was performed using particle imaging velocimetry (PIV) and Fourier transform traction cytometry (FTTC) with regularization (10^{-9}) using Fiji (29) as described previously (33). Traction forces were reconstructed at a grid spacing of 5 µm and total cellular force was calculated from the average of traction magnitudes. At least 30 cells/condition were analysed.

Migration assay and cell tracking. Transfected cells (5000 cells/well) were plated on 4-well chamber slides (Thermo Scientific™ Nunc™ Lab-Tek™ II Chamber Slide™) and imaged by using differential interference contrast (DIC) optics with a Zeiss Axiovert inverted microscope coupled to a CSUX1 spinning-disc device (Yokogawa) equipped with a 488 nm laser, sCMOS camera (Hamamatsu) and an environment chamber. Imaging was performed with a 25× oil immersion objective (Zeiss) at 37 °C, 5 % CO_2. Images were acquired at a frame rate of 1 frame/30 min for 12 h. To quantify individual cell trajectories, cells were manually tracked by using the Fiji plugin Trackmate (34). The mean distance and cell velocity were calculated by averaging the displacement (in μ) and the velocity (μm/min) between consecutive frames.

Micropattern fabrication. Micropatterned adhesive surfaces were generated using the PRIMO optical module (Alvéole, France) controlled by the Leonardo plugin (V3.3, Alveole) mounted on a Nikon TI-E inverted microscope (Nikon Instruments) equipped with a Super Plan FLuor 20x ELWD lens (Nikon) lens and a DMD-based UV (375 nm). Crossbow-shaped micropatterns (length 35 µm, width 17.5 µm, radius 17.5 µm) were projected onto plasma-cleaned (Corona Treater, ETP), PLLgPEG-passivated (0.1 mg/ml PLL-g-PEG (PLL (20)-g [3.5]- PEG (2), SuSoS) 35 mm glass-bottom dishes (Ibidi). Patterned areas were then washed multiple times with PBS and conjugated with a uniform coating of 10 µg/ml fibronectin for 1 h at 37 °C. The substrates were then washed with PBS, prior to seeding 10000 transfected fibroblast cells onto each 35 mm dish. Cells were allowed to adhere on the patterns for 16 h, at which time they fixed and processed for immunofluorescence and quantification analyses.

Immunofluorescence stainings and confocal microscopy. Cells were fixed in 4 °C paraformaldehyde, permeabilized with 0.3 % Triton X-100 in PBS, and blocked in 5 % bovine serum albumin (BSA). Samples were subsequently incubated overnight in primary antibody in 1 % BSA/0.3 % Triton X-100/PBS, followed by washing in PBS and incubation in secondary antibody in 1 % BSA/0.3 % Triton X-100/PBS. Finally, samples were mounted in Elvanol. The following antibodies were used: α-parvin (Cell Signaling; 4026; 1:100), phospho-Myosin Light Chain 2 (Thr18/Ser19) (Cell Signaling; 3674; 1:200), Paxillin (BD Transduction Laboratories; 610051; 1:300). Alexa Fluor 568 and 647 conjugated secondary antibodies (1:300, all from Invitrogen). Actin was labeled with Alexa Fluor 568 (Invitrogen; A12380 1:600), or 647-conjugated phalloidin (Invitrogen; A22287 1:100). All fluorescence images were collected by laser scanning confocal microscopy (SP8X; Leica) with Leica Application Suite software (LAS X version 2.0.0.14332), using 63x oil-immersion objective. Images where acquired at room temperature using sequential scanning of frames of 0.3 µm thick confocal planes (pinhole 1) after which 5 planes encompassing complete cell focal adhesions or actin stress fibers were projected as a maximum intensity confocal stack. Images were collected with the same settings for all samples within an experiment. Quantification of adhesion areas was performed using Fiji (29). First, ILK, or paxillin focal adhesions were identified using intensity-based thresholding (threshold area set to 10 pixels). Subsequently, focal adhesion surface area was measured by Analyze particle tools in Fiji. The cell area (in μm^2) was measured by manually tracing the cell boundary given by adhesions, phalloidin, and pMLC2 stainigs. The number of focal adhesions were normalized by the corresponding cell area.

Statistical Analysis. Statistical analyses were performed using GraphPad Prism software (GraphPad, version 8) and Python. Statistical significance was determined by the specific tests indicated in the corresponding figure legends. All experiments presented in the manuscript were repeated at least in 3 independent experiments/biological replicates. No datapoints were excluded from the analyses.

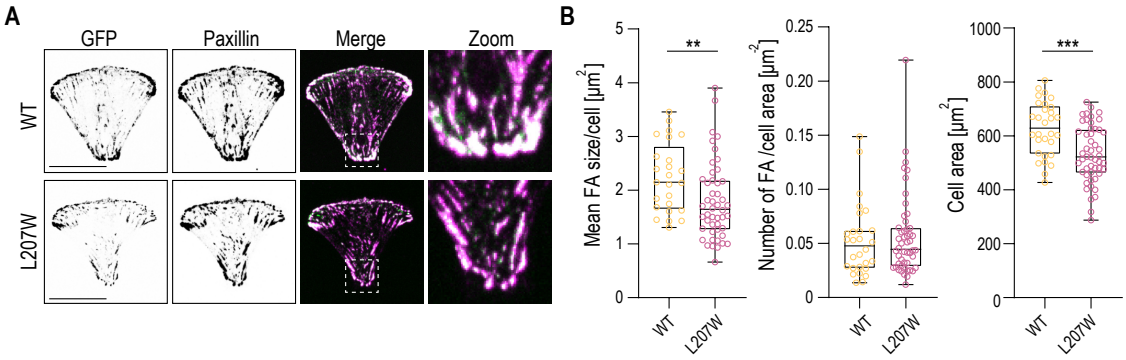

Fig. S1. (A) Representative immunofluorescence images of ILK(WT)-GFP and ILK(L207W)-GFP cells stained with paxillin on crossbow micropatterned surfaces. Paxillin localizes at focal adhesions both in ILK(WT)-GFP and ILK(L207W)-GFP cells. (B) Quantification of focal adhesion size/cell, number of focal adhesion/cell and cell area. (n > 25 cells/condition pooled across 4 independent experiments. **p= 0.0052, ***p= 0.0004, Mann-Whitney). Scale bars 20 µm.

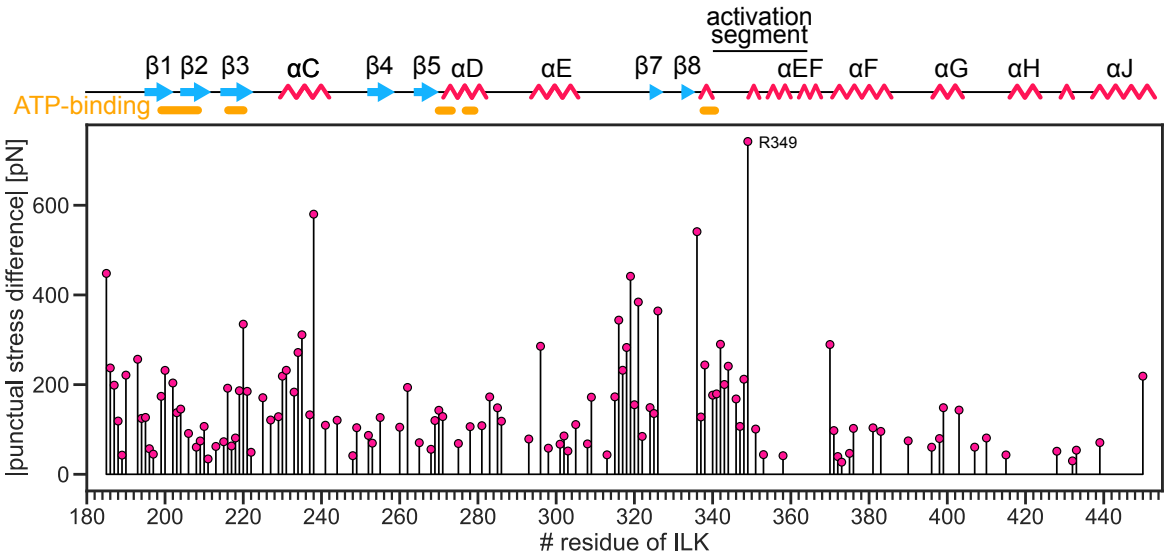

Fig. S2. Absolute differences in punctual stress between holo and apo ILK (only statistically significant differences across 20 independent simulations are shown; $p < 0.05$, Mann-Whitney test). Secondary structure elements and ATP-binding patches are indicated.

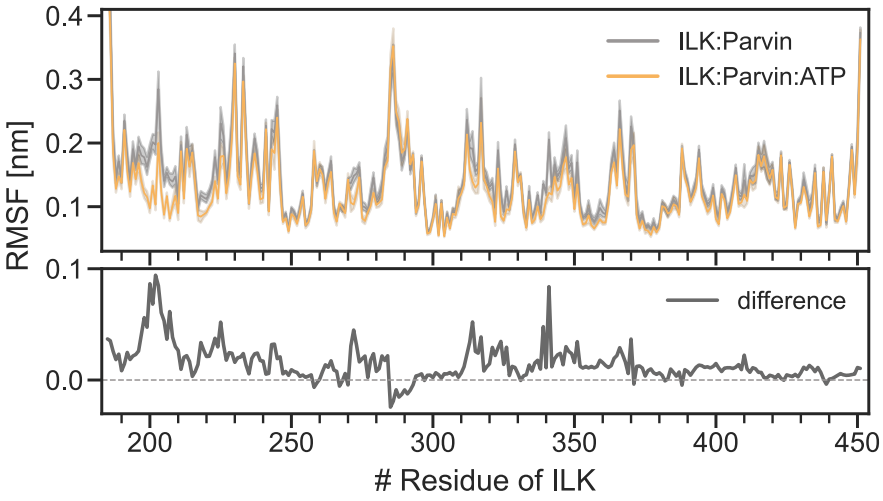

Fig. S3. Root mean square fluctuation (RMSF) of ILK holo (orange) and apo (grey) computed for the backbone atoms are shown as a function of residue number. Error bands denote the 95 % confidence interval.

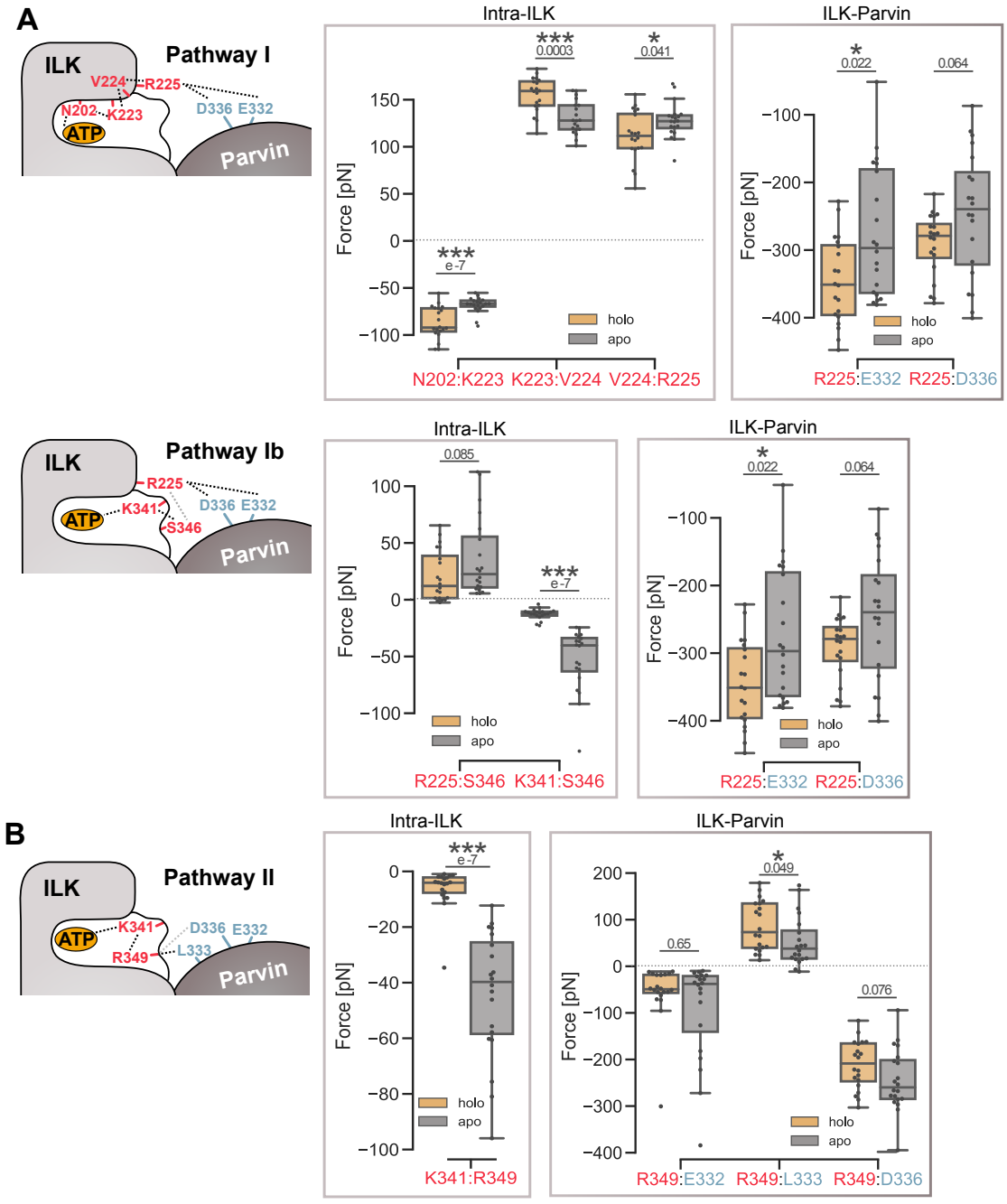

Fig. S4. ATP-dependent pathways of internal force propagation between ILK and parvin. Average pairwise forces between the indicated residue pairs are calculated from FDA for 20 individual runs compared between the apo and holo complex. Statistical significance determined by Mann-Whitney test. Positive and negative force values indicate repulsion and attraction, respectively. (A) Pathway I and pathway Ib (not quite statistically significant) involving the saltbridge-forming residue R225. (B) Pathway II involving the saltbridge-forming residue R349.

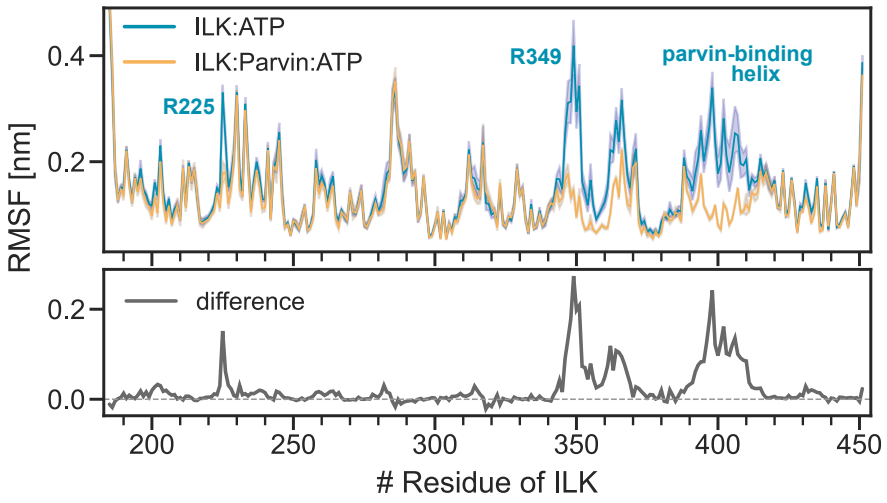

Fig. S5. Root mean square fluctuation (RMSF) of ILK in complex with parvin(orange) and without (cyan) computed for the backbone atoms are shown as a function of residue number. Error bands denote the 95 % confidence interval.

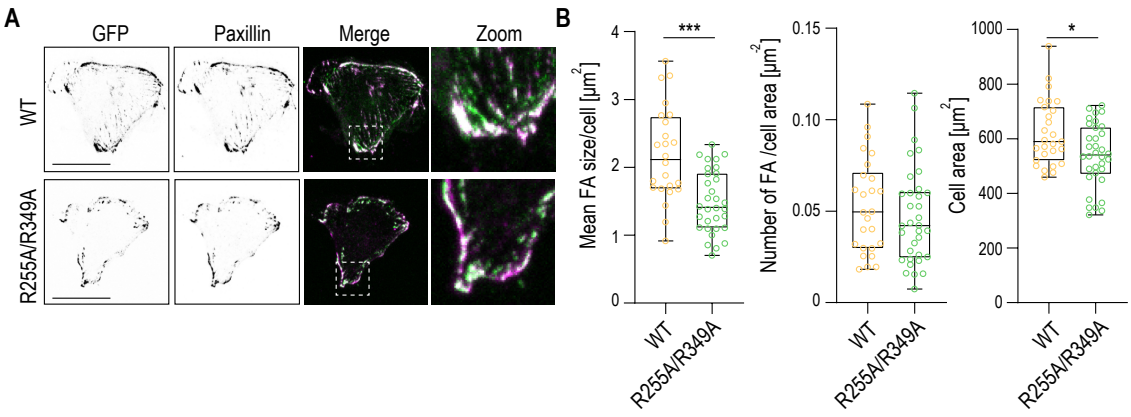

Fig. S6. (A) Representative immunofluorescence images of ILK(WT)-GFP and ILK(R255A/R349A)-GFP cells stained with paxillin on crossbow micropatterned surfaces. Paxillin localizes to focal adhesions both in ILK(WT)-GFP and ILK(R255A/R349A)-GFP cells (right panels). (B) Quantification of focal adhesion size and number (n > 24 cells/condition pooled across 4 independent experiments. ***p= 0.0001, *p= 0.0260, Mann-Whitney). Scale bars 20 µm

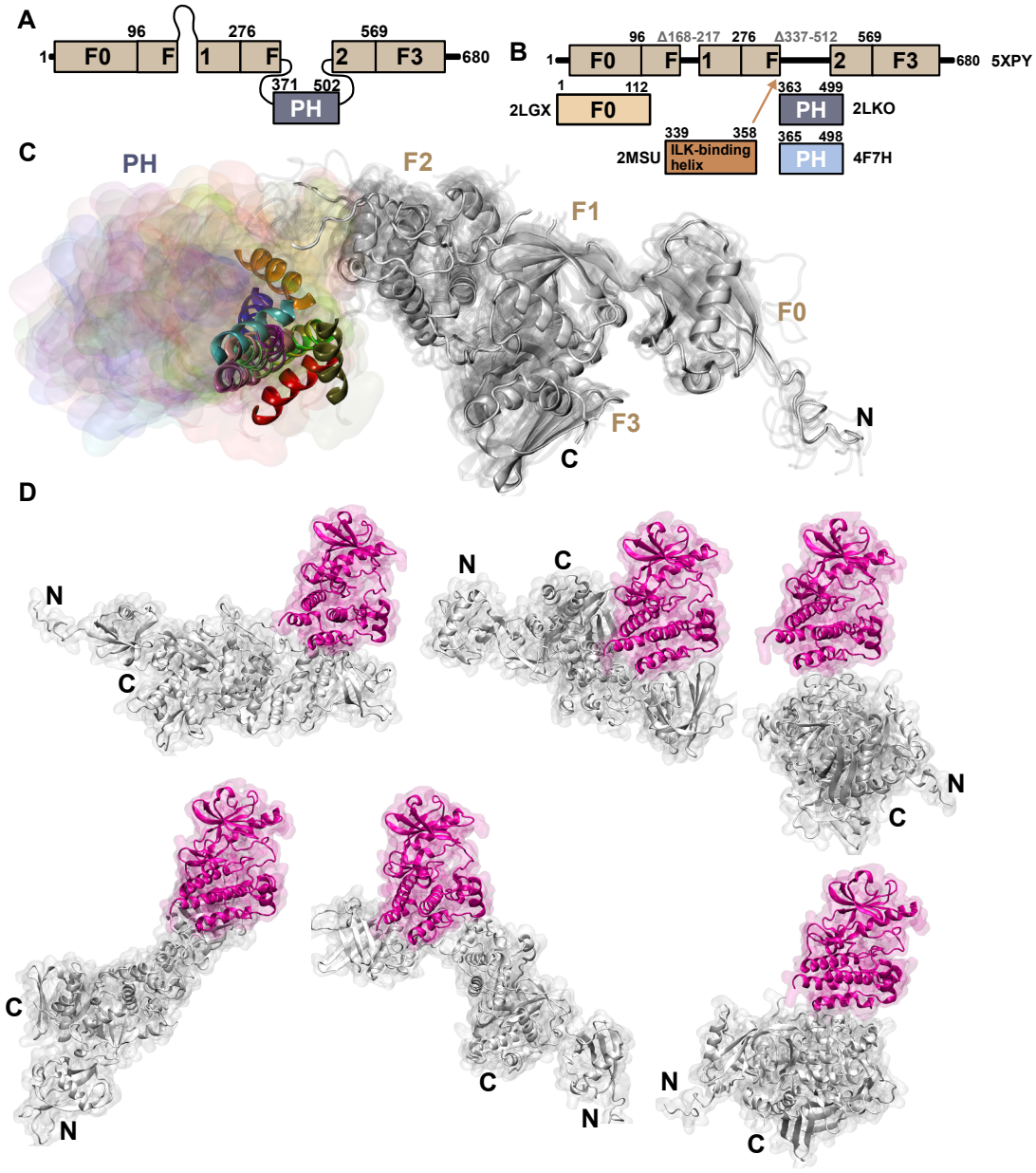

Fig. S7. Kindlin-2 modeling and ILK:kindlin-2 docking. (A) Schematic overview of full kindlin-2. (B) Schematic overview of available kindlin-2 partial crystal structures with pdb-codes. (C) Full human kindlin-2 homology models with different placements of PH-domains in surface representation in different colors. For visualization purposes one helix within the PH-domain represented in cartoon. (D) 6 exemplaric ILK:kindlin-2 docking poses from guided docking. ILK in pink and kindlin-2 in light grey. N- and C-terminus of kindlin-2 are labeled.

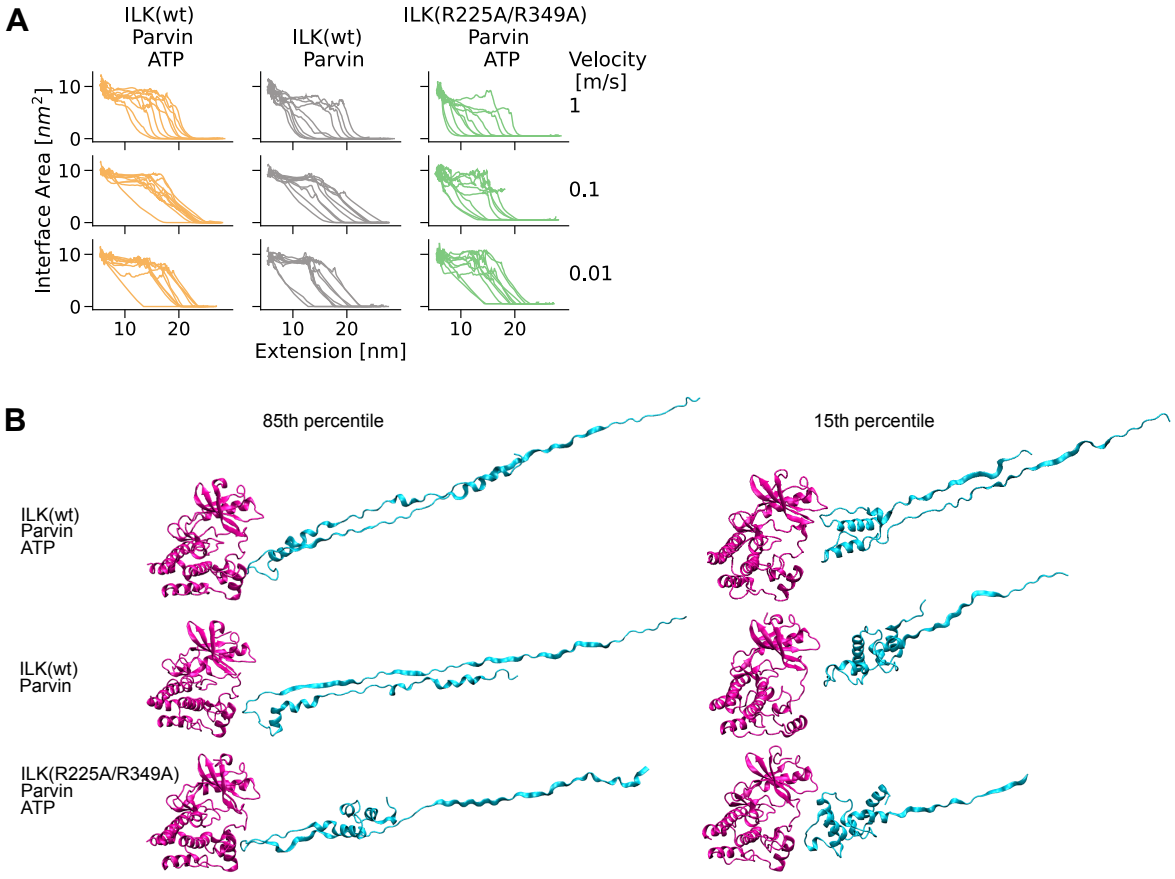

Fig. S8. ILK:parvin complex under mechanical force. (A) ILK:parvin interface area as a function of extension between the two force application patches for ILK(WT) holo and apo and ILK(R225A/R349A) at three different pulling velocities from 1 m s^{-1} to 0.01 m s^{-1}. Trajectories are smoothed with a rolling average. (B) Snapshots at the time of complex dissociation indicating the 15th and 85th percentile of each distribution.

ID1	Protein	ID2	Protein	difference pairwise force [pN]	p-value
186	ILK	187	ILK	-16.38	0.031517102
190	ILK	192	ILK	-16.93	5.89592E-05
193	ILK	217	ILK	-18.16	0.001014099
193	ILK	219	ILK	18.75	1.10447E-05
194	ILK	195	ILK	-22.79	0.004320184
194	ILK	211	ILK	-43.21	0.000509073
195	ILK	208	ILK	-18.89	1.80745E-05
197	ILK	209	ILK	44.86	0.000103734
198	ILK	199	ILK	-36.32	1.10447E-05
198	ILK	200	ILK	-26.57	6.79562E-08
199	ILK	200	ILK	99.66	6.79562E-08
199	ILK	208	ILK	-21.41	6.79562E-08
199	ILK	271	ILK	22.23	3.70512E-05
199	ILK	323	ILK	33.04	6.79562E-08
200	ILK	201	ILK	128.52	6.79562E-08
200	ILK	202	ILK	124.32	6.79562E-08
200	ILK	206	ILK	16.73	0.000247061
200	ILK	207	ILK	-57.99	2.35566E-06
200	ILK	220	ILK	85.98	6.79562E-08
200	ILK	283	ILK	18.37	5.22689E-07
200	ILK	323	ILK	-20.14	0.001782376
201	ILK	202	ILK	24.72	0.002341273
201	ILK	205	ILK	34.27	7.89803E-08
201	ILK	206	ILK	53.72	9.17277E-08
201	ILK	223	ILK	-56.78	6.0148E-07
202	ILK	204	ILK	-56.31	0.000509073
202	ILK	205	ILK	-61.46	0.000160981
202	ILK	220	ILK	62.63	3.49946E-06
202	ILK	223	ILK	-18.74	0.000115901
202	ILK	323	ILK	16.67	1.65708E-07
202	ILK	351	ILK	-31.39	0.005115262
203	ILK	204	ILK	42.72	0.000562904
203	ILK	341	ILK	15.32	0.001348582
204	ILK	220	ILK	65.63	6.79562E-08
204	ILK	223	ILK	53.39	3.29311E-05
204	ILK	341	ILK	28.09	4.16576E-05
204	ILK	345	ILK	-23.17	0.022269911
205	ILK	206	ILK	-77.52	1.23464E-07
205	ILK	221	ILK	-32.38	0.000160981
206	ILK	207	ILK	-25.08	0.003638826
206	ILK	208	ILK	-24.74	1.57567E-06
206	ILK	220	ILK	124.52	9.17277E-08
206	ILK	221	ILK	-51.21	0.00037499
206	ILK	223	ILK	83.74	2.21776E-07
207	ILK	208	ILK	145.09	9.12665E-07
207	ILK	218	ILK	77.75	6.79562E-08
207	ILK	219	ILK	57.78	1.80297E-06
207	ILK	220	ILK	123.34	1.91771E-07
208	ILK	209	ILK	-35.12	0.002798602
208	ILK	218	ILK	35.85	2.92486E-05
208	ILK	219	ILK	-63.12	7.57738E-06
209	ILK	216	ILK	21.64	2.0616E-06
209	ILK	218	ILK	28.88	1.20089E-06
209	ILK	271	ILK	-50.35	7.89803E-08
210	ILK	217	ILK	-22.44	0.000304799
211	ILK	212	ILK	24.34	0.001014099
211	ILK	216	ILK	41.67	0.016668799
212	ILK	217	ILK	-23.13	0.000144383
216	ILK	217	ILK	56.04	3.70512E-05
216	ILK	270	ILK	-17.65	0.001014099
216	ILK	271	ILK	-58.23	6.79562E-08
217	ILK	218	ILK	170.17	6.79562E-08
217	ILK	219	ILK	-25.86	6.61045E-05
217	ILK	254	ILK	21.88	0.001480977
217	ILK	268	ILK	-35.18	2.0616E-06
217	ILK	270	ILK	20.75	2.56295E-07
217	ILK	271	ILK	-21.35	0.000199707
218	ILK	219	ILK	-40.88	0.01929238
218	ILK	268	ILK	62.09	9.12665E-07
218	ILK	269	ILK	-118.51	2.56295E-07
218	ILK	271	ILK	-18.88	0.013320516
219	ILK	220	ILK	-66.66	1.57567E-06
219	ILK	267	ILK	-33.75	0.000920913
219	ILK	268	ILK	47.33	0.002341273
220	ILK	221	ILK	-16.43	0.006557193
220	ILK	266	ILK	25.09	0.000115901
220	ILK	267	ILK	-33.81	0.01929238
220	ILK	338	ILK	-30.99	0.001480977
220	ILK	339	ILK	259.93	6.79562E-08
220	ILK	340	ILK	76.02	6.79562E-08
220	ILK	341	ILK	58.81	6.79562E-08
222	ILK	223	ILK	-31.91	0.001227183
222	ILK	224	ILK	-30.25	4.53897E-07
222	ILK	264	ILK	-36.15	3.0691E-06
222	ILK	265	ILK	-22.72	0.031517102
222	ILK	342	ILK	-39.45	2.56295E-07
222	ILK	345	ILK	18.33	0.03851496
223	ILK	224	ILK	24.88	0.000338195
224	ILK	225	ILK	-16.27	0.041123594
225	ILK	227	ILK	27.78	0.031517102
225	ILK	332	Parvin	-71.31	0.022269911
226	ILK	335	Parvin	22.21	0.007113494
227	ILK	228	ILK	28.3	0.000338195

227	ILK	259	ILK	-23.45	0.036048327
229	ILK	233	ILK	23.12	0.041123594
232	ILK	259	ILK	46.86	0.000247061
234	ILK	235	ILK	-23.63	0.036048327
235	ILK	256	ILK	15.69	0.002798602
235	ILK	257	ILK	-17.18	0.036048327
235	ILK	266	ILK	33.04	0.000247061
235	ILK	267	ILK	-29.47	0.000160981
235	ILK	342	ILK	35.44	5.87357E-06
236	ILK	240	ILK	25.29	0.000160981
237	ILK	240	ILK	15.77	0.008354827
238	ILK	242	ILK	-25.11	0.002139261
239	ILK	256	ILK	37.45	3.70512E-05
239	ILK	267	ILK	-16.72	0.001348582
239	ILK	342	ILK	16.47	0.00604033
240	ILK	243	ILK	31.4	0.000274511
250	ILK	337	ILK	-22.47	0.022269911
251	ILK	269	ILK	-27.93	0.004702533
251	ILK	272	ILK	34.49	7.57738E-06
252	ILK	269	ILK	24.74	0.033717669
253	ILK	267	ILK	28.54	2.92486E-05
254	ILK	268	ILK	-86.48	0.000920913
255	ILK	267	ILK	24.3	0.000199707
256	ILK	267	ILK	-22.03	0.020734594
257	ILK	265	ILK	21.2	0.00556046
258	ILK	259	ILK	-32.62	0.000920913
258	ILK	262	ILK	-35.17	0.000415502
259	ILK	265	ILK	-18.15	0.004320184
262	ILK	264	ILK	-17.29	4.16576E-05
264	ILK	266	ILK	18.83	0.003966239
267	ILK	268	ILK	-43.51	0.000460073
267	ILK	338	ILK	-57.57	3.41558E-07
268	ILK	269	ILK	-34.37	0.011432829
269	ILK	270	ILK	-50.5	2.92486E-05
270	ILK	271	ILK	53.32	0.000144383
271	ILK	272	ILK	-34.58	0.009045397
272	ILK	275	ILK	-52.32	3.29311E-05
272	ILK	326	ILK	78.23	2.35566E-06
272	ILK	327	ILK	-38.48	5.16578E-06
272	ILK	328	ILK	-26.61	3.70512E-05
272	ILK	334	ILK	-23.08	0.000338195
273	ILK	274	ILK	73.03	0.000247061
273	ILK	275	ILK	-19.96	6.61045E-05
276	ILK	277	ILK	22.45	0.027483422
276	ILK	278	ILK	70.97	2.68977E-06
276	ILK	322	ILK	19.16	0.000835717
276	ILK	325	ILK	34.57	0.006557193
276	ILK	326	ILK	83.08	5.16578E-06
277	ILK	281	ILK	44.46	0.022269911
277	ILK	322	ILK	-24.4	0.025639272
277	ILK	325	ILK	-36.37	0.001348582
278	ILK	283	ILK	-32.07	0.000460073
278	ILK	323	ILK	-48.33	9.27796E-05
279	ILK	284	ILK	22.05	0.003966239
282	ILK	283	ILK	36.73	0.005115262
282	ILK	389	ILK	22.03	0.04986369
283	ILK	323	ILK	44.59	0.002139261
296	ILK	300	ILK	-38.04	0.023903146
296	ILK	451	ILK	27.75	0.003638826
298	ILK	301	ILK	20.67	0.033717669
300	ILK	304	ILK	-18.82	0.014363848
300	ILK	332	ILK	16.48	0.046791615
301	ILK	381	ILK	18.72	0.043880384
305	ILK	306	ILK	-17.13	0.007711805
307	ILK	310	ILK	16.37	0.043880384
307	ILK	311	ILK	-32.93	0.003336179
308	ILK	309	ILK	22.85	0.002798602
308	ILK	335	ILK	17.76	0.000835717
311	ILK	315	ILK	-19.88	0.023903146
312	ILK	317	ILK	15.55	0.022207185
315	ILK	340	ILK	16.19	0.031517102
317	ILK	340	ILK	23.39	0.009786487
317	ILK	366	ILK	26.95	0.001782376
317	ILK	374	ILK	54.25	0.036048327
318	ILK	324	ILK	-33.84	0.006557193
318	ILK	335	ILK	-41.81	0.000509073
318	ILK	340	ILK	21.33	0.025639272
318	ILK	341	ILK	27.66	0.011432829
319	ILK	324	ILK	37	0.000686822
319	ILK	339	ILK	-32.15	0.000562904
320	ILK	321	ILK	67.16	0.000144383
320	ILK	377	ILK	52.01	0.000757881
320	ILK	378	ILK	-29.61	0.003056629
321	ILK	323	ILK	60.47	0.001115947
321	ILK	325	ILK	-32.49	0.013320516
321	ILK	339	ILK	26.37	0.001782376
321	ILK	355	ILK	64.66	0.001480977
321	ILK	381	ILK	26.23	0.000686822
322	ILK	323	ILK	-48.68	0.01929238
322	ILK	324	ILK	-28.73	0.000247061
322	ILK	381	ILK	32.78	0.002341273
322	ILK	384	ILK	85	4.54008E-06
323	ILK	324	ILK	-54.77	0.001115947
323	ILK	326	ILK	52.39	2.56295E-07
323	ILK	339	ILK	63.3	0.000415502
323	ILK	355	ILK	-22.34	0.000129405

323	ILK	384	ILK	67.31	0.023903146
324	ILK	335	ILK	-16.84	0.007711805
324	ILK	336	ILK	62.02	0.04986369
325	ILK	326	ILK	-35.23	0.029440884
325	ILK	334	ILK	-21	0.007113494
326	ILK	327	ILK	49.2	0.003638826
326	ILK	333	ILK	28.94	0.001625258
326	ILK	334	ILK	30.84	0.031517102
326	ILK	336	ILK	19.12	0.041123594
326	ILK	339	ILK	-30.83	6.0148E-07
328	ILK	332	ILK	-36.78	0.009045397
335	ILK	336	ILK	94.34	0.000115901
336	ILK	339	ILK	34.29	0.001227183
337	ILK	338	ILK	-54.5	0.003336179
337	ILK	339	ILK	79.45	0.000144383
338	ILK	339	ILK	55.18	0.001782376
338	ILK	340	ILK	-119.49	1.91771E-07
338	ILK	341	ILK	-33.41	6.79562E-08
339	ILK	341	ILK	-113.25	0.000222203
340	ILK	342	ILK	-41.42	2.0616E-06
341	ILK	345	ILK	54.02	2.0616E-06
341	ILK	346	ILK	40.31	6.79562E-08
341	ILK	349	ILK	37.75	1.91771E-07
341	ILK	351	ILK	-15.24	3.70512E-05
342	ILK	345	ILK	122.12	1.20089E-06
343	ILK	345	ILK	-42.76	5.89592E-05
345	ILK	346	ILK	63.7	0.000222203
348	ILK	349	ILK	-54.93	0.001953348
349	ILK	333	Parvin	32.97	0.04986369
355	ILK	356	ILK	26.1	0.036048327
355	ILK	377	ILK	59.59	1.59972E-05
355	ILK	384	ILK	48.48	0.03851496
359	ILK	360	ILK	-24.99	0.000509073
364	ILK	311	Parvin	-19.72	0.007711805
365	ILK	366	ILK	-16.05	0.003336179
366	ILK	370	ILK	21.95	0.016668799
370	ILK	373	ILK	20.31	0.020734594
370	ILK	374	ILK	-97.79	0.004702533
372	ILK	433	ILK	16.4	0.013320516
376	ILK	377	ILK	22.8	0.006557193
380	ILK	381	ILK	29.64	0.027483422
380	ILK	383	ILK	26.85	0.025639272
390	ILK	391	ILK	35.67	0.000103734
392	ILK	393	ILK	-19.31	0.031517102
397	ILK	398	ILK	-16.7	0.010581211
397	ILK	401	ILK	-15.1	0.002341273
399	ILK	403	ILK	33.51	0.001953348
400	ILK	401	ILK	32.92	0.003966239
400	ILK	404	ILK	-24.26	0.00604033
408	ILK	409	ILK	-16.62	0.015478602
432	ILK	436	ILK	-16.32	0.03851496
436	ILK	437	ILK	-17.5	0.033717669
450	ILK	451	ILK	-33.86	0.000415502
254	Parvin	362	Parvin	17.78	0.01929238
285	Parvin	287	Parvin	31.15	0.046791615
291	Parvin	352	Parvin	16.99	0.000103734
292	Parvin	294	Parvin	25.06	0.002139261
296	Parvin	300	Parvin	-17.37	0.015478602
299	Parvin	300	Parvin	40.85	0.001480977
308	Parvin	313	Parvin	19.37	0.005115262
309	Parvin	311	Parvin	34.06	0.004702533
310	Parvin	312	Parvin	-18.48	0.001625258
328	Parvin	332	Parvin	21.7	0.043880384
331	Parvin	334	Parvin	-15.69	0.001782376
331	Parvin	335	Parvin	31.26	0.006557193
332	Parvin	335	Parvin	-52.9	1.80745E-05
333	Parvin	335	Parvin	-21.47	0.013320516
333	Parvin	336	Parvin	-25.48	0.027483422
333	Parvin	337	Parvin	39.47	0.001953348
334	Parvin	335	Parvin	49.79	0.003056629
334	Parvin	336	Parvin	-16.11	0.007113494
334	Parvin	339	Parvin	23.5	0.027483422
336	Parvin	337	Parvin	-33.96	0.002798602
336	Parvin	338	Parvin	27.38	0.020734594
339	Parvin	340	Parvin	29.53	0.008354827
343	Parvin	344	Parvin	17.88	0.010581211
344	Parvin	345	Parvin	36.64	0.000686822
345	Parvin	346	Parvin	28.86	0.017938613
347	Parvin	348	Parvin	-19.89	0.020734594
347	Parvin	351	Parvin	21.97	0.009786487
348	Parvin	349	Parvin	31.93	0.000686822
350	Parvin	352	Parvin	27.12	0.007711805
354	Parvin	355	Parvin	21.76	0.04986369
356	Parvin	357	Parvin	15.97	0.036048327
357	Parvin	358	Parvin	23.12	0.046791615
359	Parvin	360	Parvin	23.94	0.009786487
364	Parvin	368	Parvin	55.99	0.001625258
367	Parvin	368	Parvin	21.08	0.041123594

Table S1. Differences in pairwise forces between the holo and apo state calculated from FDA (n = 20 independent trajectories, p <0.05, Mann-Whitney).

Movie S1. ILK large-scale motions captured by PC1 ("inter-lobe wringing motion") extracted from PCA. Interpolation between the extreme conformations (red and blue) along PC1. ILK is shown as C-α traces. See also Figure 1D.

Movie S2. ILK large-scale motions captured by PC2 ("lobe clamping motion") extracted from PCA. Interpolation between the extreme conformations (red and blue) along PC2. ILK is shown as C-α traces. See also Figure 1D.

Movie S3. Representative movies of ILK(WT)-GFP (left) and ILK(L207W)-GFP cells (right) shown in Fig. 2D and imaged on 8 kPa substrates. Arrowheads and asterisks (in magenta) indicate adhesion growth and adhesion disassembly, respectively. Frame rate 1 min/frame. Scale bar 20 µm.

Movie S4. Representative movies of ILK(WT)-GFP (left) and ILK(L207W)-GFP cells (right) shown in Fig. 2D and imaged on 40 kPa substrates. Arrowheads and asterisks (in magenta) indicate adhesion growth and adhesion disassembly, respectively. Frame rate 1 min/frame. Scale bar 20 µm.

Movie S5. Representative movies of ILK(WT)GFP (left) and ILK(R255A/R349A)-GFP cells (right) shown in Fig. 4D and imaged on 8 kPa substrates. Arrowheads and asterisks (in magenta) indicate adhesion growth and adhesion disassembly, respectively. Frame rate 1 min/frame. Scale bar 20 µm.

Movie S6. Representative movies of ILK(WT)GFP (left) and ILK(R255A/R349A)-GFP cells (right) shown in Fig. 4D and imaged on 40 kPa substrates. Arrowheads and asterisks (in magenta) indicate adhesion growth and adhesion disassembly, respectively. Frame rate 1 min/frame. Scale bar 20 µm.

Movie S7. Example of ILK(pink):parvin(cyan) dissociation after significant parvin unfolding in force-probe MD simulations as exemplified here by the holo complex, where this behavior is more commonly observed. Residues investigated in this study are shown in ball-and-stick representation, the pulling patch for constant velocity pulling with 1 m/s is indicated in dark grey.

Movie S8. Example of ILK(pink):parvin(cyan) dissociation after marginal parvin unfolding in force-probe MD simulations as exemplified here by the apo complex, where this behavior is more commonly observed. Residues investigated in this study are shown in ball-and-stick representation, the pulling patch for constant velocity pulling with 1 m/s is indicated in dark grey.

Movie S9. Example of ILK(pink):parvin(cyan) dissociation with no parvin unfolding in force-probe MD simulations as exemplified here by the ILK(R225A/R349A):parvin holo complex. Residues investigated in this study are shown in ball-and-stick representation, the pulling patch for constant velocity pulling with 1 m/s is indicated in dark grey.

Movie S10. Real time imaging of ILK-/-GFP cell migration. Representative movie of ILK-/-GFP cells cultured on glass and captured by spinning disc time-lapse microscopy at initial (0 h) and 12 h time. Trajectories in magenta and green. Frame rate 30 min/frame. Scale bar 20 µm.

Movie S11. Real time imaging of ILK(WT)-GFP cell migration. Representative movie of ILK(WT)-GFP cells cultured on glass and captured by spinning disc time-lapse microscopy at initial (0 h) and 12 h time. Trajectory in magenta and green. Frame rate 30 min/frame. Scale bar 20 µm.

Movie S12. Real time imaging of ILK(L207W)-GFP cell migration. Representative movie of ILK(L207W)-GFP cells cultured on glass and captured by spinning disc time-lapse microscopy at initial (0 h) and 12 h time. Trajectory in magenta. Frame rate 30 min/frame. Scale bar 20 µm.

Movie S13. Real time imaging of ILK(R255A/R349A)-GFP cell migration. Representative movie of ILK(R255A/R349A)-GFP cells cultured on glass and captured by spinning disc time-lapse microscopy at initial (0 h) and 12 h time. Trajectories in magenta and green. Frame rate 30 min/frame. Scale bar 20 µm.

References

1. K Fukuda, S Gupta, K Chen, C Wu, J Qin, The pseudoactive site of ilk is essential for its binding to alpha-parvin and localization to focal adhesions. *Mol. cell* **36**, 819–830 (2009).
2. J Vaynberg, et al., Non-catalytic signaling by pseudokinase ilk for regulating cell adhesion. *Nat. communications* **9**, 4465 (2018).
3. MJ Abraham, et al., Gromacs: High performance molecular simulations through multi-level parallelism from laptops to supercomputers. *SoftwareX* **1-2**, 19–25 (2015).
4. RB Best, G Hummer, Optimized molecular dynamics force fields applied to the helix-coil transition of polypeptides. *The journal physical chemistry. B* **113**, 9004–9015 (2009).

5. AE Aliev, et al., Motional timescale predictions by molecular dynamics simulations: case study using proline and hydroxyproline sidechain dynamics. *Proteins* **82**, 195–215 (2014).
6. WL Jorgensen, J Chandrasekhar, JD Madura, RW Impey, ML Klein, Comparison of simple potential functions for simulating liquid water. *The J. Chem. Phys.* **79**, 926–935 (1983).
7. KL Meagher, LT Redman, HA Carlson, Development of polyphosphate parameters for use with the amber force field. *J. computational chemistry* **24**, 1016–1025 (2003).
8. B Hess, P-lincs: A parallel linear constraint solver for molecular simulation. *J. chemical theory computation* **4**, 116–122 (2008).
9. G Bussi, D Donadio, M Parrinello, Canonical sampling through velocity rescaling. *The J. Chem. Phys.* **126**, 014101 (2007).
10. M Parrinello, A Rahman, Polymorphic transitions in single crystals: A new molecular dynamics method. *J. Appl. Phys.* **52**, 7182–7190 (1981).
11. T Darden, D York, L Pedersen, Particle mesh ewald: An n x log(n) method for ewald sums in large systems. *The J. Chem. Phys.* **98**, 10089–10092 (1993).
12. H Li, et al., Structural basis of kindlin-mediated integrin recognition and activation. *Proc. Natl. Acad. Sci. United States Am.* **114**, 9349–9354 (2017).
13. K Fukuda, et al., Molecular basis of kindlin-2 binding to integrin-linked kinase pseudokinase for regulating cell adhesion. *The J. biological chemistry* **289**, 28363–28375 (2014).
14. J Liu, et al., Structural basis of phosphoinositide binding to kindlin-2 protein pleckstrin homology domain in regulating integrin activation. *The J. biological chemistry* **286**, 43334–43342 (2011).
15. Y Liu, Y Zhu, S Ye, R Zhang, Crystal structure of kindlin-2 ph domain reveals a conformational transition for its membrane anchoring and regulation of integrin activation. *Protein & cell* **3**, 434–440 (2012).
16. HD Perera, et al., Membrane binding of the n-terminal ubiquitin-like domain of kindlin-2 is crucial for its regulation of integrin activation. *Struct. (London, Engl. : 1993)* **19**, 1664–1671 (2011).
17. EF Pettersen, et al., Ucsf chimera–a visualization system for exploratory research and analysis. *J. computational chemistry* **25**, 1605–1612 (2004).
18. P Di Tommaso, et al., T-coffee: a web server for the multiple sequence alignment of protein and rna sequences using structural information and homology extension. *Nucleic acids research* **39**, W13–7 (2011).
19. B Webb, A Sali, Comparative protein structure modeling using modeller. *Curr. protocols bioinformatics* **54**, 5.6.1–5.6.37 (2016).
20. GCP van Zundert, et al., The haddock2.2 web server: User-friendly integrative modeling of biomolecular complexes. *J. molecular biology* **428**, 720–725 (2016).
21. YA Kadry, C Huet-Calderwood, B Simon, DA Calderwood, Kindlin-2 interacts with a highly-conserved surface of ilk to regulate focal adhesion localization and cell spreading. *J. cell science* **131** (2018).
22. S Lorenz, et al., Structural analysis of the interactions between paxillin ld motifs and alpha-parvin. *Struct. (London, Engl. : 1993)* **16**, 1521–1531 (2008).
23. X Wang, et al., The structure of alpha-parvin ch2-paxillin ld1 complex reveals a novel modular recognition for focal adhesion assembly. *The J. biological chemistry* **283**, 21113–21119 (2008).
24. F Eisenhaber, P Lijnzaad, P Argos, C Sander, M Scharf, The double cubic lattice method: Efficient approaches to numerical integration of surface area and volume and to dot surface contouring of molecular assemblies. *J. Comput. Chem.* **16**, 273–284 (1995).
25. W Humphrey, A Dalke, K Schulten, Vmd: visual molecular dynamics. *J. molecular graphics* **14**, 33–8, 27–8 (1996).
26. CC David, DJ Jacobs, Principal component analysis: a method for determining the essential dynamics of proteins. *Methods molecular biology (Clifton, N.J.)* **1084**, 193–226 (2014).
27. BI Costescu, F Gräter, Time-resolved force distribution analysis. *BMC biophysics* **6**, 5 (2013).
28. K Radovanac, et al., Stabilization of integrin-linked kinase by the hsp90-chip axis impacts cellular force generation, migration and the fibrotic response. *The EMBO journal* **32**, 1409–1424 (2013).
29. J Schindelin, et al., Fiji: an open-source platform for biological-image analysis. *Nat. methods* **9**, 676–682 (2012).
30. RJ Pelham, Yl Wang, Cell locomotion and focal adhesions are regulated by substrate flexibility. *Proc. Natl. Acad. Sci. United States Am.* **94**, 13661–13665 (1997).
31. ME Berginski, SM Gomez, The focal adhesion analysis server: a web tool for analyzing focal adhesion dynamics. *F1000Research* **2**, 68 (2013).
32. M Dembo, Yl Wang, Stresses at the cell-to-substrate interface during locomotion of fibroblasts. *Biophys. journal* **76**, 2307–2316 (1999).
33. Q Tseng, et al., A new micropatterning method of soft substrates reveals that different tumorigenic signals can promote or reduce cell contraction levels. *Lab on a chip* **11**, 2231–2240 (2011).
34. JY Tinevez, et al., Trackmate: An open and extensible platform for single-particle tracking. *Methods (San Diego, Calif.)* **115**, 80–90 (2017).